SCIENTIFIC REPORTS

OPEN

Improved electrochemical properties of $LiNi_{0.91}Co_{0.06}Mn_{0.03}O_2$ cathode material via Li-reactive coating with metal phosphates

Received: 25 April 2017
Accepted: 27 June 2017
Published online: 2 August 2017

Kyoungmin Min[1], Kwangjin Park[2], Seong Yong Park[1], Seung-Woo Seo[1], Byungjin Choi[2] & Eunseog Cho[1]

Ni-rich layered oxides are promising cathode materials due to their high capacities. However, their synthesis process retains a large amount of Li residue on the surface, which is a main source of gas generation during operation of the battery. In this study, combined with simulation and experiment, we propose the optimal metal phosphate coating materials for removing residual Li from the surface of the Ni-rich layered oxide cathode material $LiNi_{0.91}Co_{0.06}Mn_{0.03}O_2$. First-principles-based screening process for 16 metal phosphates is performed to identify an ideal coating material that is highly reactive to Li_2O. By constructing the phase diagram, we obtain the equilibrium phases from the reaction of coating materials and Li_2O, based on a database using a DFT hybrid functional. Experimental verification for this approach is accomplished with $Mn_3(PO_4)_2$, $Co_3(PO_4)_2$, $Fe_3(PO_4)_2$, and $TiPO_4$. The Li-removing capabilities of these materials are comparable to the calculated results. In addition, electrochemical performances up to 50 charge/discharge cycles show that Mn-, Co-, Fe-phosphate materials are superior to an uncoated sample in terms of preventing capacity fading behavior, while $TiPO_4$ shows poor initial capacity and rapid reduction of capacity during cycling. Finally, Li-containing equilibrium phases examined from XRD analysis are in agreement with the simulation results.

There has been increasing demand for lithium ion batteries (LIBs) for application in electric devices such as mobile phones and electrical vehicles. To achieve high energy density and long-term cyclability in LIBs, the use of transition metal (TM)-based oxide cathode materials could be an ideal option because their optimal composition can provide large capacity, low manufacturing cost, and great rate capability[1–4]. Nickel-rich nickel-cobalt-manganese oxide (termed Ni-rich NCM) is a class of promising materials that can satisfy those needs, but they suffer from several types of degradation behaviors such as phase transformation and gas generation[5–7].

To mitigate degradation behaviors in layered oxide cathode materials thus enhancing the electrochemical performance, the surface modification method, *i.e.*, surface coating, has been suggested to provide a physical barrier at the surface of the cathode and prevent the direct contact between active materials and electrolytes. For example, many metal phosphate (MP) materials are suggested as effective coating materials such as MPO_4 (M = Al, Fe, Ce, and Sr)[8,9], $Ni_3(PO_4)_2$[10], $Mn_3(PO_4)_2$[11], $M_3(PO_4)_2$ (M = Zn and Mg)[12], and Zr-phosphate [13] for cathode materials such as $LiCoO_2$ (LCO), $LiNi_{0.9}Co_{0.1}O_2$, $LiNi_{0.8}Co_{0.15}Al_{0.05}O_2$ (NCA), $LiNi_{0.6}Co_{0.2}Mn_{0.2}O_2$, and $LiNi_{0.8}Co_{0.15}Mn_{0.05}O_2$. In spite of their effectiveness in improving the capacity retention rate, this type of coating approach in principle has drawbacks: 1) Li ion diffusion during electrochemical cycling can be impeded, 2) residual Li still needs to be washed, which requires an additional step during synthesis, and 3) this process can degrade battery performance[14–16]. Li impurities, which are residues on the surface of the cathode formed after initial synthesis, are a major source of gas generation, resulting in swelling behavior inside the battery pack[14,17]. The excessive amount of Li used as a prerequisite for achieving sufficient capacity with Ni-rich cathode materials is a source of these impurities[17,18]. Previous studies demonstrated that residual Li (such as LiOH and Li_2CO_3) can

[1]Platform Technology Lab, Samsung Advanced Institute of Technology, 130 Samsung-ro, Suwon, Gyeonggi-do, 16678, Republic of Korea. [2]Energy Lab, Samsung Advanced Institute of Technology, 130 Samsung-ro, Suwon, Gyeonggi-do, 16678, Republic of Korea. Kyoungmin Min and Kwangjin Park contributed equally to this work. Correspondence and requests for materials should be addressed to K.M. (email: kmin.min@samsung.com) or E.C. (email: eunseog.cho@samsung.com)

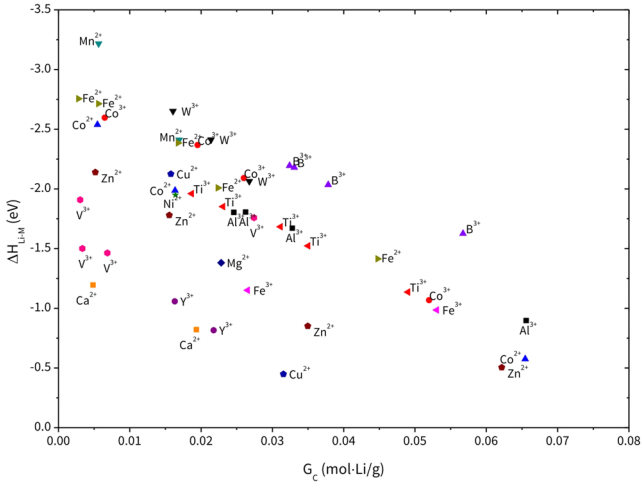

Figure 1. Overall design chart for the reaction between metal phosphate and Li_2O.

initiate the decomposition reaction with electrolytes at the interface, leading to the evolution of gas species such as CO_2, O_2, N_2, and CO[14–16].

Application of Li-containing phosphates such as $LiNiPO_4$[19], $Li_3V_2(PO_4)_3$[20], and $LiAlTi(PO_4)_3$[21] coating materials has been recommended to alleviate the problem of constricted Li ion diffusion, and they have been shown to improve the rate capability and prevent capacity fading during cycling. Another approach has been suggested to eliminate the two concerns simultaneously, *i.e.*, finding coating materials that can directly react with residual Li so that they can be transformed to Li-containing phases and in parallel the amount of Li residue is reduced. For example, Kim *et al.* suggested using $Co_3(PO_4)_2$ as a Li-reacting coating material that can be converted to $LiCoPO_4$ during annealing[16]. $AlPO_4$ was also demonstrated to be functional from this perspective by forming Li_3PO_4 and $LiAlO_2$ after its reaction with Li residues[22]. Jo *et al.* proved that phosphoric acid (H_3PO_4) can be changed to Li_3PO_4 via a Li-reactive mechanism[23]. However, only a few attempts have been made with this concept, which makes it difficult to choose the optimal MP coating materials for this purpose. It is worth noting that a computational approach has been successfully applied by Wolverton's group to search for optimal coating materials to scavenge hydrofluoric acid (HF)[24, 25] and interfacial stability between coating and cathode materials[26]. In this regard, the computational aid is promising for examining and screening MP materials that are highly reactive to Li residues and can form subsequent Li-containing equilibrium phases. The amount of Li residue increases for Ni-rich cathode materials; hence, more surface area is covered with residual Li[17]. Therefore, MP materials are likely to first react with residual Li and form Li-containing structures; remaining unreacted materials still can function as coating material by blocking the direct exposure of the cathode material to the electrolyte.

In this study, we implement a computational framework to propose the optimal MP coating material for removing residual Li from the surface of Ni-rich layered oxide cathode material $LiNi_{0.91}Co_{0.6}Mn_{0.3}O_2$ (NCM) by employing first-principles calculations on 16 MP materials. The results are validated with experiments measuring the reduction in the amount of Li residue after applying the coating materials. We also perform electrochemical cycling tests to clarify which of the coating materials is more effective in preventing capacity fading. Finally, the equilibrium phases obtained from experiment are compared to those from the phase diagrams obtained by calculation.

Results and Discussion

Design chart and analysis. The overall reaction behavior between MP and Li_2O in terms of reaction enthalpy ($\Delta H_{Li\text{-}M}$). and gravimetric capacity (G_C) is shown in Fig. 1 (The complete list of reaction equations is shown in Table S.2 in SI). Each MP material has several possible reactions depending on the amount used. For example, $Fe_3(PO_4)_2$ can undergo five reactions at various molar ratios from 0.12 to 2 relative to Li_2O. Among the possible reactions with one material, it is energetically preferable when a larger weight of coating materials is applied. Hence, this relation complicates finding the optimal coating material holding both strengths, *i.e.*, the largest reaction energy and the least weight.

To provide comprehensive understanding of the performance of each MP material, we further analyzed the design chart by extracting data and sorting them with respect to their competencies. Two types of data analysis were performed, *i.e.*, the descending order of $\Delta H_{Li\text{-}M}$ and G_C values and their corresponding G_C and $\Delta H_{Li\text{-}M}$ values (denoted G_C' and $\Delta H_{Li\text{-}M}'$), respectively. The descending order means that the results are sorted according to the largest value among several possible reaction equations containing each material. Meanwhile, corresponding values (*e.g.*, $\Delta H_{Li\text{-}M}'$) indicate $\Delta H_{Li\text{-}M}$ of the reaction when sorted in descending order of G_C, and *vice versa*. The complete list is shown in Table S.3.

First, the descending order of $\Delta H_{Li\text{-}M}$ obtained in Fig. 2a exhibits that $Mn_3(PO_4)_2$ is the most energetically preferable, followed by $Fe_3(PO_4)_2$, $W(PO_4)_2$, $CoPO_4$, $Co_3(PO_4)_2$, etc. The most preferable reaction from each material is shown in equation number 1 in Table S.2. In terms of G_C (shown in Fig. 2b), $AlPO_4$ is calculated to be the most efficient followed by $Co_3(PO_4)_2$, $Zn_3(PO_4)_2$, BPO_4, $FePO_4$, etc.

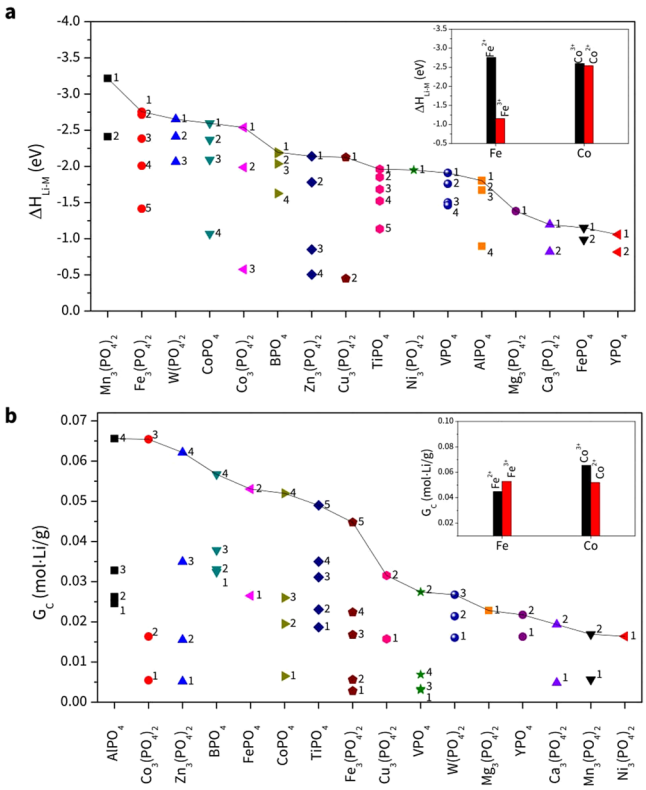

Figure 2. The descending orders of (**a**) $\Delta H_{Li\text{-}M}$ and (**b**) G_C, and (inset) comparison between materials having the same metal element for the reaction between metal phosphate and Li_2O. Each number in (**a**) and (**b**) denotes the reaction equation number.

Several significant findings can be addressed based on the above analysis. First, the MP materials positioned at higher ranks in terms of $\Delta H_{Li\text{-}M}$ generally exhibit poor efficiency, *i.e.*, they require a larger weight to achieve that reaction. For example, the most Li-reactive material ($Mn_3(PO_4)_2$) is placed at 11th in order of G_C' and at 15th in the descending order of G_C. However, it is worthwhile to mention that its $\Delta H_{Li\text{-}M}'$ is still the highest. This result indicates that it is desirable to use $Mn_3(PO_4)_2$ when its higher reactivity to Li_2O is required, but the weight of the coating material is not a critical condition to meet. Likewise, $W(PO_4)_2$ is placed 3rd in the descending order of ΔH_{Li} and its corresponding ΔH_{Li} with respect to the descending order of G_C is 2nd, which indicates that its reaction with Li_2O is highly preferable. However, as shown with $Mn_3(PO_4)_2$, this material requires a large weight because its G_C is positioned 8th from the corresponding order of $\Delta H_{Li\text{-}M}$ and 11th in the descending order of G_C values (Table S.3).

As discussed earlier, it is difficult to find coating materials satisfying both criteria of reactivity and gravimetric efficiency. Among 16 calculated materials, $Co_3(PO_4)_2$ and BPO_4 reveal moderate capabilities for both constraints. For example, $\Delta H_{Li\text{-}M}$ of $Co_3(PO_4)_2$ is ranked 5th and its G_C is also positioned high (2nd). This means that this MP material can have good performance depending on which constraint is more important. BPO_4 exhibits modest performance from all perspectives; all of its capabilities are within the 6th place of the 16 MP materials and its capability is not sensitive to the amount used. Its $\Delta H_{Li\text{-}M}$ value is positioned 6th and its corresponding G_C is 5th while its G_C is ranked 4th and its corresponding $\Delta H_{Li\text{-}M}$ is 5th.

Since two of the metal elements (Fe and Co) can take multiple oxidation states (*e.g.*, Co is in the +2 and +3 states in $Co_3(PO_4)_2$ and $CoPO_4$, respectively), it is important to compare the performances of those species, as shown in the Inset of Fig. 2. In the case of Fe-based phosphate, the comparison shows that $Fe_3(PO_4)_2$ exhibits better performance than $FePO_4$. More specifically, it is more energetically preferable than $FePO_4$; its $\Delta H_{Li\text{-}M}$ value is positioned 2nd while that of $FePO_4$ is at the 15th position in the descending order. However, $FePO_4$ exhibits better gravimetric efficiency (G_C is ranked 5th) than that of $Fe_3(PO_4)_2$ (ranked 8th). Hence, one needs to choose Fe-P based on the purpose of use. Reactivities of Co-based phosphates are almost the same ($CoPO_4$ and $Co_3(PO_4)_2$ ranked 4th and 5th, respectively) but the G_C value of $Co_3(PO_4)_2$ (ranked 2nd) is better than that of $CoPO_4$ (ranked 6th); hence using $Co_3(PO_4)_2$ will be more satisfactory.

Li-removal capacity: simulation vs. experiment. Based on the screened results from the above calculations, we chose four of the 16 MP materials for experimental validation. $Fe_3(PO_4)_2$, $Co_3(PO_4)_2$, and $Mn_3(PO_4)_2$) were chosen because their reaction with Li_2O is energetically superior to the others; their $\Delta H_{Li\text{-}M}$ values are all within the top 5 of 16 MP materials for reaction #1. $TiPO_4$ was also chosen to verify the general trend of calculated results because its $\Delta H_{Li\text{-}M}$ is positioned 9th.

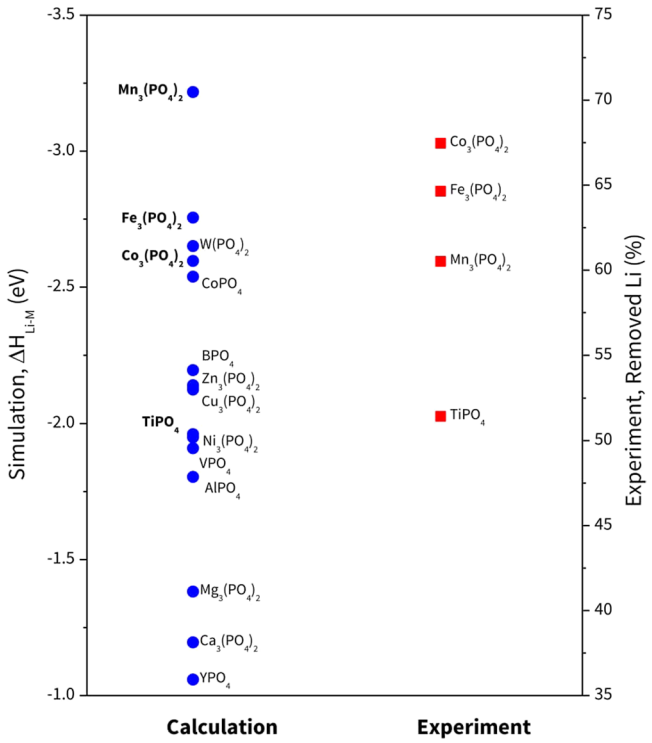

Figure 3. Comparison of Li-removal reactivity from calculations and experiment. Calc denotes that their values are obtained from the descending order of $\Delta H_{Li\text{-}M}$. MPs enclosed with squares indicate the materials that are compared with experiment.

First, the amounts of Li removed/reacted due to reactions after the Li-reactive coating process were measured (Table S.4). The amounts of LiOH and Li_2CO_3 were measured using titration. This is because during the coating process at 720 °C, these Li compounds are transformed to Li_2O then they revert to LiOH and Li_2CO_3 due to reaction with H_2O and CO_2 impurities[17,27,28]. The result indicates that $Co_3(PO_4)_2$ can remove almost 70% of residual Li of the uncoated cathode, and Fe- and Mn-P are also shown to be effective (67% and 64% of Li residues were reduced, respectively). Meanwhile, $TiPO_4$ exhibited moderate performance; 51% of Li was removed. We associate this result with the simulations by comparing their $\Delta H_{Li\text{-}M}$ values from the most preferable reaction of each material (reaction #1, the case for Calc[a]) as shown in Fig. 3. We think this comparison is reasonable because a larger $\Delta H_{Li\text{-}M}$ value from simulations means that this reaction is more likely to happen, so it can remove more residual Li during the experiment. The general trend is reasonably in agreement, *i.e.*, coating materials with better experimental Li removal capacities (Co-, Fe-, and Mn-P) also have larger values of $\Delta H_{Li\text{-}M}$, while $TiPO_4$ exhibited poorer performance and has a lower value of $\Delta H_{Li\text{-}M}$.

Effect of coating on the electrochemical performance of cathode. The energy dispersive X-ray spectrometric (EDS) elemental maps of the metal elements in the MPs are shown in Fig. 4a. Unlike the pristine structure shown in Figure S.3, it clearly confirms the presence of these coating materials, which are distributed on the surface of the primary and the secondary particles of the NCM. The HAADF (high-angle annular dark-field imaging)-STEM (scanning transmission electron microscopy) images and the quantitative EDS mapping data for all of elements are presented in the SI.

To understand the effect of coating material on the electrochemical performance of NCM cathodes, the Coulombic efficiency, initial capacity, and capacity retention rate (CRR) during cycling were measured (Table 1). The Coulombic efficiency values exhibited by all the coating materials were superior to those of the bare material. Their 1st capacity at 0.2 C rate exhibited that the $Co_3(PO_4)_2$-coated sample possessed the largest capacity (219.08 mAh/g), even larger than that of the bare (uncoated) material (217.47 mAh/g). This unusual behavior can be attributed to the formation of $LiCoO_2$ phase on the surface after reacting with Li compounds, which is suggested from the current simulation result (further discussion will be provided in the following section).

Other coating materials had initial capacity reduced by around 10 mAh/g relative to the uncoated case. The capacities of all coated materials dropped significantly (around 30 mAh/g) due to the faster C-rate after measuring the 1st capacity at 1 C rate capacity. This behavior was more severe in the case of $TiPO_4$; the capacity decreased from 208.53 to 143.05 mAh/g after changing the rate from 0.2 C to 1 C.

The trend and values of capacity and CRR for all materials up to 50 cycles with 1 C rate are presented in Fig. 4b,c and Table 1. $Co_3(PO_4)_2$ coating exhibited the best performance considering its 1st cycle capacity and the CRR value (76.68%); both properties were larger than those of other materials considered in this study. $Fe_3(PO_4)_2$ and $Mn_3(PO_4)_2$ coating materials also demonstrated great performance in terms of CRR (77.16% and 73.08%, respectively), which are larger than that of the uncoated case (72.98%). Although the 1 C capacities with $Fe_3(PO_4)_2$

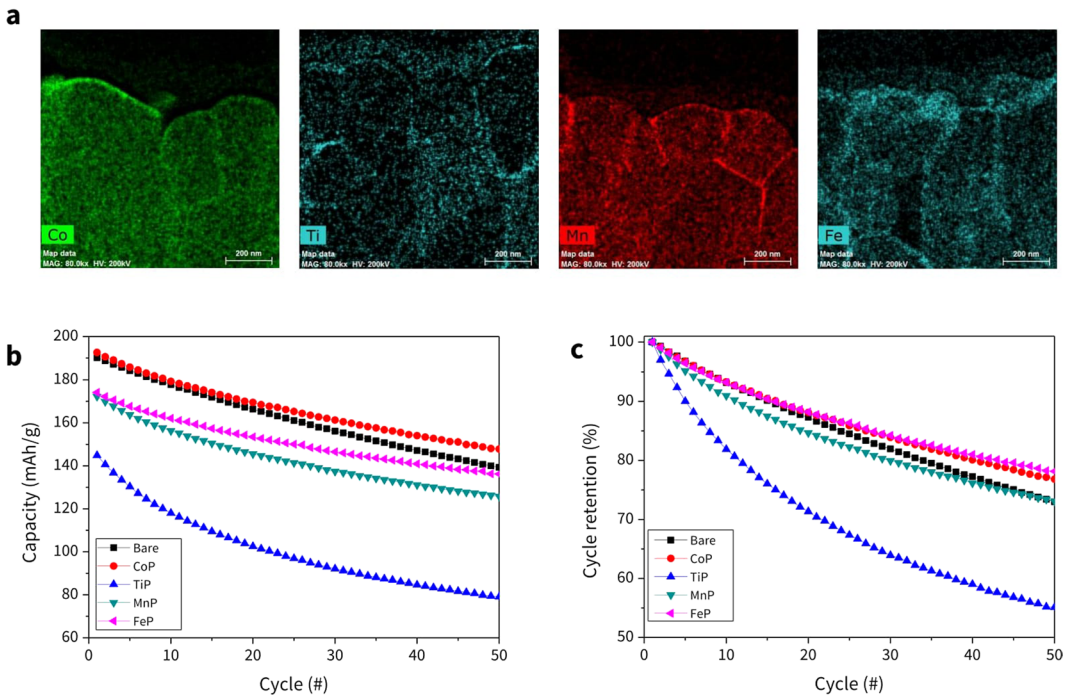

Figure 4. (**a**) EDS elemental mapping of corresponding metal element for Co-, Ti-, Mn-, and Fe-P. (**c**) The variation of the initial capacity and (**d**) the capacity retention rate during 50 cycles for NCM and NCM coated with Co-, Ti-, Mn-, and Fe-P.

	Initial capacity at 0.1 C (mAh/g)		Coulombic efficiency (%)	2nd capacity at 0.2 C (mAh/g)	1 C capacity (mAh/g)	Cycle retention (%)
Bare (Uncoated)	273.65	223.20	81.56	217.47	189.69	72.98
$Co_3(PO_4)_2$	243.85	224.53	92.08	219.08	191.53	76.68
$TiPO_4$	242.13	217.18	89.69	208.53	143.05	55.12
$Mn_3(PO_4)_2$	239.14	212.77	88.97	206.92	171.16	73.08
$Fe_3(PO_4)_2$	238.92	211.64	88.58	205.84	171.9	77.16

Table 1. Initial capacity at 0.1 C, Coulombic efficiency, 2nd capacity at 0.2 C, at 1 C, and the cycle retention rates for uncoated and coated NCM cathodes.

and $Mn_3(PO_4)_2$ coatings are initially smaller than that of the uncoated case, their capacities are expected to be conserved better during cycling considering their CRR values and the trend of curves, compared to that from the uncoated case (Fig. 4b,c). The $TiPO_4$ coating exhibits poor performance on all electrochemical properties; its CRR rate is very low (55.12%) and hence, using this material is not desirable. In summary, Co-, Fe-, and Mn-P materials can reduce significant amounts of Li residue and they also exhibit great electrochemical properties as coating materials, while $TiPO_4$ is neither effective at removing Li residues nor at conserving the capacity of the cathode during cycling.

Equilibrium phase verification. To elucidate the equilibrium phase formed on the surface of the cathode after residual Li-removal by coating materials, a simulated experiment was performed by reacting MP materials directly with the Li compounds, followed by comparison of their phases with those obtained in the calculated phase diagram.

First, we constructed the $Co_3(PO_4)_2$ - Li_2O - O_2 phase diagram and obtained the reaction product, as shown in Fig. 5a,b. The stable products generated between MP and Li_2O are important to understand the direct reaction mechanism between the coating materials and residual Li. Since the experiment is usually performed under an O_2 environment, it is also critical to provide an O_2 axis and investigate the products that newly emerge. It should be noted that in general more phases are available under O_2 flow. The complete list of phases available from simulations of other coating materials is tabulated in Table 2.

The calculated equilibrium phase of $Co_3(PO_4)_2$ when the molar ratio of 2:1 is $LiCoPO_4$ (reaction #O1), exhibiting good agreement with the experimental result. A previous study also demonstrated that $LiCoPO_4$ phase can be formed on the surface of NCA cathode material after Li-reactive reaction with $Co_3(PO_4)_2$ coating material[16]. $LiMnP_2O_7$ or $Li_2MnP_2O_7$ phase can be generated from $Mn_3(PO_4)_2$ coating material after its Li-reactive reaction when the molar ratio is 2:1 or 1:1, respectively; the latter form shows agreement with experiment. Finally, the

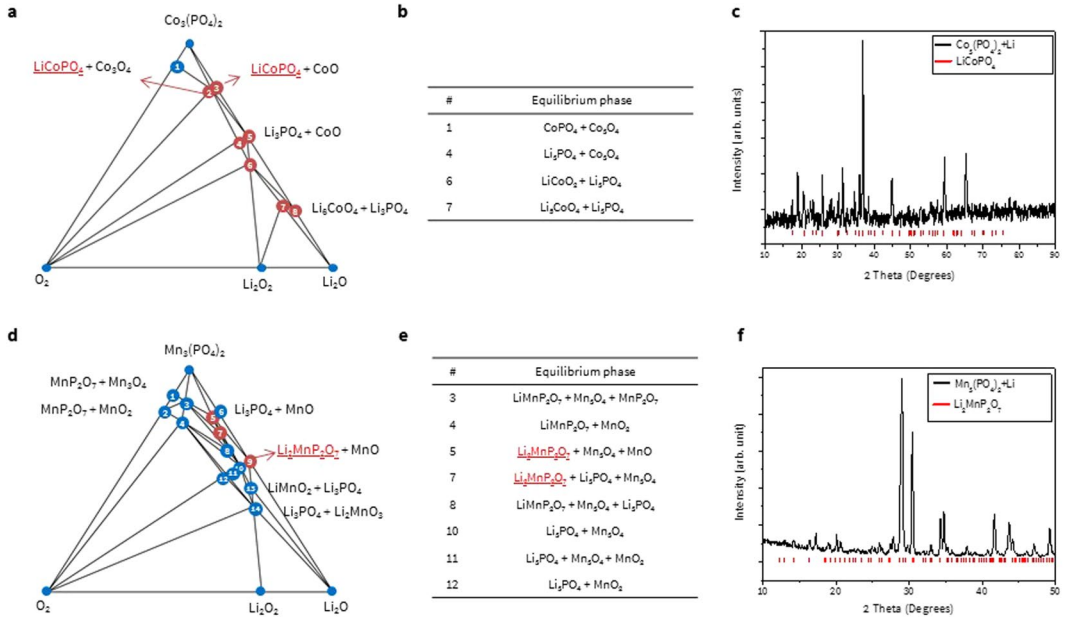

Figure 5. (**a**,**d**) Phase diagram, (**b**,**e**) equilibrium phase information, and (**c**,**f**) XRD pattern of $Co_3(PO_4)_2$ and $Mn_3(PO_4)_2$ coating materials after reacting with Li residue (black) and peak information of the discovered phase. Blue and red circles in the phase diagram represent the stable phase and the stable phase confirmed from XRD analysis, respectively.

Coating Materials	Equilibrium phases	
	MP - Li_2O	MP - Li_2O - O_2
$Mn_3(PO_4)_2$	$Li_2MnP_2O_7$, Li_3PO_4	$LiMnP_2O_7$, $Li_2MnP_2O_7$, $LiMnO_2$, Li_2MnO_3, Li_3PO_4
$Fe_3(PO_4)_2$	$Li_2Fe_3P_4O_{14}$, $LiFePO_4$, $LiFeO_2$, Li_3PO_4,	$LiFe(PO_3)_4$, $Li_2Fe_3(P_2O_7)_2$, $LiFePO_4$, $LiFeP_2O_7$, $LiFeO_2$, Li_2FeO_3, Li_5FeO_4, Li_3PO_4
$W(PO_4)_2$	Li_4WO_5, Li_2WO_4, Li_3PO_4	n/a
$CoPO_4$	$LiCoPO_4$,$LiCoO_2$, Li_5CoO_4, Li_3PO_4	n/a
$Co_3(PO_4)_2$	$LiCoPO_4$, Li_6CoO_4, Li_3PO_4	Li_6CoO_4, $LiCoPO_4$, $LiCoO_2$, Li_5CoO_4, Li_3PO_4
BPO_4	$Li_3B_7O_{12}$, $Li_2B_4O_7$, $LiBO_2$, Li_3BO_3, Li_3PO_4	n/a
$Zn_3(PO_4)_2$	$LiZnPO_4$, $Li_{10}Zn_4O_9$, Li_6ZnO_4, Li_3PO_4	n/a
$Cu_3(PO_4)_2$	Li_3CuO_3, LiCuO, Li_3PO_4	Li_3CuO_3, Li_3PO_4
$TiPO_4$	$LiTi_2O_4$, Li_2TiO_3, Li_3PO_4	$LiTi_2(PO_4)_3$, $LiTi_2O_4$, Li_2TiO_3, $LiTi_2O_4$, Li_4TiO_4, Li_3PO_4
$Ni_3(PO_4)_2$	Li_3PO_4	$LiNi_2O_4$, Li_2NiO_3, Li_3PO_4
VPO_4	$LiVP_2O_7$, Li_3PO_4	$LiVP_2O_7$, $LiVO_3$, Li_3VO_4, Li_3PO_4
$AlPO_4$	$LiAlO_2$, $LiAl_5O_8$, Li_5AlO_4, Li_3PO_4	n/a
$Mg_3(PO_4)_2$	Li_3PO_4	n/a
$Ca_3(PO_4)_2$	Li_3PO_4	n/a
$FePO_4$	$LiFeO_2$, Li_5FeO_4, Li_3PO_4	Li_2FeO_3, Li_3PO_4, Li_5FeO_4, Li_2O_2, Li_3PO_4
YPO_4	$LiYO_2$, Li_3PO_4	n/a

Table 2. Equilibrium phases formed from the reaction between MP-Li_2O and MP-Li_2O-O_2 based on phase diagrams. Underlined phases denote that they are found both with and without O_2 environment.

equilibrium phases can be supported by previous reference in the case of $AlPO_4$. When $AlPO_4$ is coated on the surface of LCO cathode, it can be transformed to Li_3PO_4 and $LiAlO_2$ phases due to reaction with Li residues[22], which agrees with current calculations.

Figure 6 provides further validation for the Fe- and Ti-P coating materials. For $Fe_3(PO_4)_2$, it is important to mention that since the molar ratio of coating materials to residual Li used in the simulated experiment for XRD analysis (molar ratio is 2:1) are much larger than in the actual coating (1 wt% of NCM, molar ratio around 0.3:1), the existing phases after coating can be different. For example, when the molar ratio of 2:1 $Fe_3(PO_4)_2$ to Li_2O is provided in a simulated experiment, the possible reaction is #O2 or #O3 in Table S.5, whose equilibrium phase is $Li_2Fe_3(P_2O_7)_2$ or $LiFeP_2O_7$, respectively (the experimentally observed phase is $LiFeP_2O_7$, as shown in Fig. 6c). However, when a smaller molar ratio of coating material is provided, the Li-reacted phase could vary (such as $LiFePO_4$, Li_3PO_4, Li_2FeO_3, etc.) depending on the amount of coating material. Similarly, the possible phases for

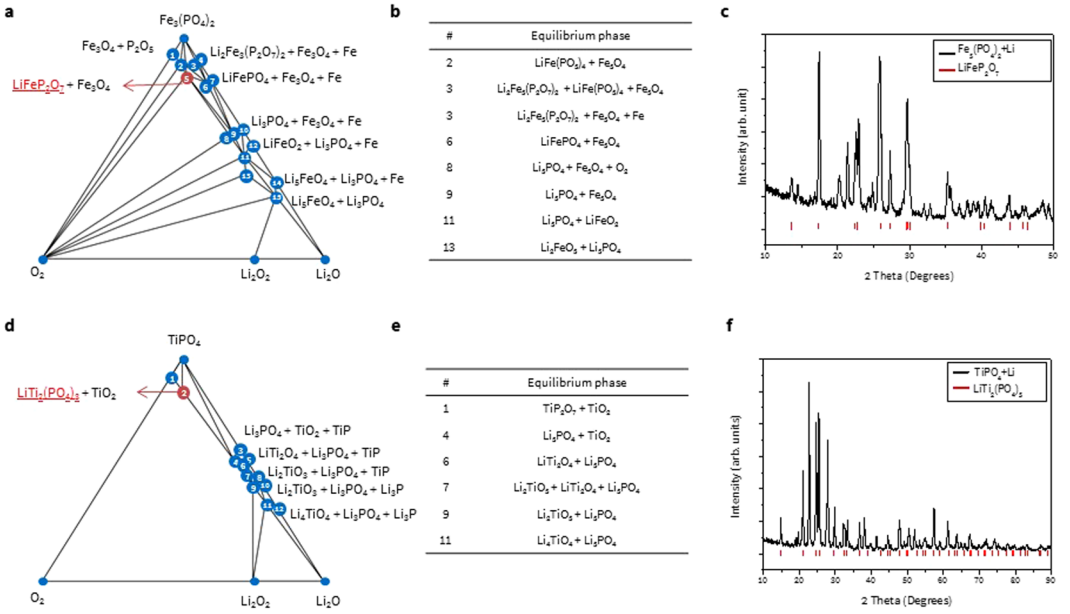

Figure 6. (**a**,**d**) Phase diagram, (**b**,**e**) equilibrium phase information, and (**c**,**f**) XRD pattern of $Fe_3(PO_4)_2$ and $TiPO_4$ coating materials after reacting with Li residue (black) and peak information of the discovered phase. Blue and red circles in the phase diagram represent the stable phase and the stable phase confirmed from XRD analysis, respectively.

$TiPO_4$ after reaction with Li_2O can be $LiTi_2(PO_4)_3$ or Li_3PO_4 provided the molar ratio (2:1) is between #O1 (6:1) and #O2 (0.67:1) in Table S.5 (the former phase matches the simulated experiment in Fig. 6f); when a smaller molar ratio is provided, the phase could be Li_3PO_4, $LiTi_2O_4$, etc.

In summary, Li-containing phases formed from the simulated experiment were verified by comparing with the phases predicted by calculations with molar ratios based on the phase diagram. This indicates that the phase on the cathode surface can be tuned by altering the amount of coating material with respect to that of the Li residue.

Conclusions

In this study, we implemented a screening process by constructing phase diagrams based on a first-principles approach to propose the optimal phosphate coating materials that can effectively reduce the amount of residual Li (Li_2O). Verification of this framework was achieved by performing experiments measuring the remaining Li residue and obtaining electrochemical properties during cycling. Based on the $\Delta H_{Li\text{-}M}$ values from calculations, the MP coating materials $Co_3(PO_4)_2$, $Mn_3(PO_4)_2$, $Fe_3(PO_4)_2$, and $TiPO_4$ were chosen for experimental validation. It was found that the order of reactivity of coating materials for removing Li residues was in good agreement between simulations and experiments; Co-, Mn-, and Fe-P materials exhibited great Li-removal capability. To further confirm the functionalities of coating material on the improvement of cycle life, electrochemical cycling tests showed that Co-, Mn-, and Fe-P materials are effective coating materials for the prevention of capacity fading behaviors. $Co_3(PO_4)_2$ showed the largest initial capacity among the coating materials tested and its capacity was conserved well, indicating that it would be an ideal coating material for NCM cathode material. In addition, experimental products generated after the reaction of MP and Li were confirmed by comparison with predicted phases obtained from the phase diagram based on calculations.

Methods

Computational details: Screening process. We identified the optimal coating materials based on results from first-principles calculations by constructing the phase diagram to obtain Li-containing equilibrium phases. A total of 16 MP materials were calculated with the information of reaction enthalpy ($\Delta H_{Li\text{-}M}$) and gravimetric capacity (G_C) when they react with residual Li. $\Delta H_{Li\text{-}M}$ indicates the reaction energy when reactants are changed to products while G_C is the weight of coating material required for the removal of one mole of Li_2O. Gaseous products generated during this reaction can be disregarded because the Li-reactive coating process occurs at 700 °C; these gases can be removed during ventilation. The overall screening process, computational details, and the database for the formation energy of all materials used in this study are adopted from our previous work[29]. Here is a brief overview of the computational approach.

1) Formation energy values of all related structures were obtained to construct the database. To improve the accuracy of these energy values, density functional theory calculations using the Vienna *ab initio* simulation package (VASP)[30,31] with HSE06 hybrid functional were employed[32,33].
2) The phase diagrams for MP-Li_2O-O_2 were constructed and equilibrium (energetically preferable) phases examined.

3) The reaction equations were obtained based on step 2) with their reaction products and enthalpies.
4) The design chart containing $\Delta H_{Li\text{-}M}$ and G_C information was constructed to identify the ideal MP coating material for removal of Li residue.

Unlike our preceding study, here we focused on the reaction of MP with Li_2O instead of LiOH and Li_2CO_3. This is because the decomposition reactions of both LiOH and Li_2CO_3 to Li_2O could occur beyond the temperature of 700 °C (the coating process in this study was performed at 720 °C), following reactions based on the JANAF-NIMS thermochemistry data table[34] and post-processed data from our previous study[28],

$$2LiOH(s) \rightarrow Li_2O(s) + H_2O(g) \quad (1)$$

$$Li_2CO_3(s) \rightarrow Li_2O(s) + CO_2(g) \quad (2)$$

LiOH starts to decompose to Li_2O around 300 °C under average ambient humidity. Decomposition of Li_2CO_3 could be dominant below 700 °C with the partial pressure of CO_2 in the coating environment.

Experimental methods. *Sample preparation and coating process.* NCM was synthesized by means of a co-precipitation method. Suitable amounts of precursors of Ni, Mn, and Co (Ni:Co:Mn = 91:6:3) were dissolved in deionized (DI) water and stirred to obtain a homogeneous solution. Next, a chelating agent (NH_4OH) with a stoichiometric amount of NaOH solution was added to achieve co-precipitated $(NiMnCo)(OH)_2$ after sufficient stirring. The precipitate was co-ground with a stoichiometric amount of LiOH and calcined at 750 °C under O_2 flow.

Cobalt nitrate ($Co(NO_3)_3{\cdot}9H_2O$), aluminum nitrate ($Al(NO_3)_3{\cdot}9H_2O$), iron(III) nitrate ($Fe(NO_3)_3{\cdot}9H_2O$), manganese(II) nitrate tetrahydrate ($Mn(NO_3)_2{\cdot}4H_2O$), titanium(IV) oxyacetylacetonate ($C_{10}H_{14}O_5Ti$), and diammonium phosphate ($(NH_4)_2HPO_4$, termed DMP) were used as source materials to form MP for the surface modification. Assuming the formation of 1 wt% of MP (NCM = 30 g) on the surface of NCM, the amounts of metal and phosphate source were calculated as listed in Table S.1 (Supplementary Information, SI). The coating process was achieved as follows. The stoichiometric metal source was dissolved in DI water. After the NCM powder was suspended in the metal solution, DMP solution was slowly added with a dropper. The solution was then stirred and dried at 120 °C until the solvent evaporated completely. The resulting coated NCM substrate was heated at 720 °C for 5 h in flowing O_2 gas (30 liter/min).

Structural analysis for Li-reactive coating. Simulated experiments were carried out using the same coating materials composed of metal nitrates (the equivalent source as that used for surface coating), DMP, and Li residues (LiOH and Li_2CO_3). It was assumed that during the coating process, the Li residues and coating materials (excluding NCM) participated in the reaction. The molar ratio of coating material to Li residue was 2:1. After each material was mixed, the mixture was heated to 720 °C under O_2 for 5 h.

The material was analyzed after heat treatment using X-ray powder diffraction (XRD) to identify the equilibrium phases in the coating materials. Structural examination of the sample was performed by an X-ray diffractometer using Cu-K_α radiation with a scan speed of 0.02° per minute between 10° and 90° at an applied potential of 40 kV and current of 40 mA.

Microstructure analysis was performed using double Cs corrected transmission electron microscopy (TEM, FEI titan cubed 60–300). The composition of the particle surface was confirmed by energy dispersive spectroscopy (EDS, Bruker Super-X).

Electrochemical measurements. Composite positive electrodes containing 92 wt% active material, 4 wt% Denka black, and 4 wt% polyvinylidene difluoride (PVdF) were fabricated and pasted on the current collector (aluminum foil). The electrodes were dried at 120 °C under vacuum and then pressed. Metallic lithium was used as the counter electrode. The electrolyte solution consisted of 1.0 M $LiPF_6$ dissolved in a solution of fluoroethylene carbonate (FEC) and dimethylene carbonate (DMC). CR2032-type coin cells were assembled in a dry room. The cells were discharged and charged galvanostatically and the measurements were conducted in triplicate at each test condition. The loading level for the active ingredient was 10 mg/cm^2. The cycling performance of the cells was measured at 25 °C at a charge/discharge rate of 1 C.

The amount of Li residue was estimated by the titration method. Since Li_2CO_3 and LiOH are soluble in water, most of the Li sources were assumed to originate from these compounds. The total Li (ppm) was calculated from the following equation.

$$\text{Total Li(ppm)} = \frac{2 \times \text{atomic weight of Li}}{\text{molar weight of } Li_2CO_3} \times Li_2CO_3\text{(ppm)} + \frac{\text{atomic weight of Li}}{\text{molar weight of LiOH}} \times \text{LiOH(ppm)} \quad (3)$$

Data availability. The datasets generated during and/or analyzed during the current study are available from the corresponding author on reasonable request.

References

1. Chen, W. *et al*. Controlled synthesis of concentration gradient LiNi0.84Co0.10Mn0.04Al0.02O1.90F0.10 with improved electrochemical properties in Li-ion batteries. *RSC Adv.* **6**, 58173–58181 (2016).
2. Bak, S.-M. *et al*. Structural Changes and Thermal Stability of Charged LiNi x Mn y Co z O 2 Cathode Materials Studied by Combined *In Situ* Time-Resolved XRD and Mass Spectroscopy. *ACS Appl. Mater. Interfaces* **6**, 22594–22601 (2014).
3. Chen, W. *et al*. Controlled synthesis of spherical hierarchical LiNi1−x−yCoxAlyO2 (0 < x, y < 0.2) via a novel cation exchange process as cathode materials for High-Performance Lithium Batteries. *Electrochim. Acta* **190**, 932–938 (2016).
4. Chen, W. *et al*. Aluminum Insertion-Induced Enhanced Performance of Li(Ni0.83-xCo0.10Mn0.07Aly)O2 Microspheres for Lithium-Ion Batteries Design. *ChemElectroChem* **1**, 601–610 (2014).
5. Liu, W. *et al*. Nickel-Rich Layered Lithium Transitional-Metal Oxide for High-Energy Lithium-Ion Batteries. *Angew. Chemie Int. Ed.* 4440–4457, doi:10.1002/anie.201409262 (2015).
6. Min, K. *et al*. A comparative study of structural changes in lithium nickel cobalt manganese oxide as a function of Ni content during delithiation process. *J. Power Sources* **315**, 111–119 (2016).
7. Min, K., Seo, S.-W., Song, Y. Y., Lee, H. S. & Cho, E. A first-principles study of the preventive effects of Al and Mg doping on the degradation in LiNi0.8Co0.1Mn0.1O2 cathode materials. *Phys. Chem. Chem. Phys.* **19**, 1762–1769 (2017).
8. Kim, J., Noh, M., Cho, J., Kim, H. & Kim, K.-B. Controlled Nanoparticle Metal Phosphates (Metal = Al, Fe, Ce, and Sr) Coatings on LiCoO2 Cathode Materials. *J. Electrochem. Soc.* **152**, A1142–A1148 (2005).
9. Lee, H. *et al*. Structural Characterization of the Surface-Modified Li x Ni0.9Co0.1O2 Cathode Materials by MPO4 Coating (M = Al, Ce, SrH, and Fe) for Li-Ion Cells. *J. Electrochem. Soc.* **153**, A781–A786 (2006).
10. Lee, D.-J., Scrosati, B. & Sun, Y.-K. Ni3(PO4)2-coated Li[Ni0.8Co0.15Al0.05]O2 lithium battery electrode with improved cycling performance at 55 °C. *J. Power Sources* **196**, 7742–7746 (2011).
11. Cho, W. *et al*. Investigation of new manganese orthophosphate Mn3(PO4)2 coating for nickel-rich LiNi0.6Co0.2Mn0.2O2 cathode and improvement of its thermal properties. *Electrochim. Acta* **198**, 77–83 (2016).
12. Eom, J. & Cho, J. M3 (PO4) 2-Nanoparticle-Coated LiCoO2 vs LiCo0.96M0.04O2 (M = Mg and Zn) on Electrochemical and Storage Characteristics. *J. Electrochem. Soc.* **155**, A201–A205 (2008).
13. Park, K. *et al*. Enhancement in the electrochemical performance of zirconium/phosphate bi-functional coatings on LiNi0.8Co0.15Mn0.05O2 by the removal of Li residuals. *Phys. Chem. Chem. Phys*. doi:10.1039/C6CP05286J (2016).
14. Xiong, X. *et al*. Washing effects on electrochemical performance and storage characteristics of LiNi0.8Co0.1Mn0.1O2 as cathode material for lithium-ion batteries. *J. Power Sources* **222**, 318–325 (2013).
15. Kim, Y. Encapsulation of LiNi0.5Co0.2Mn0.3O2 with a thin inorganic electrolyte film to reduce gas evolution in the application of lithium ion batteries. *Phys. Chem. Chem. Phys.* **15**, 6400–6405 (2013).
16. Kim, Y. & Cho, J. Lithium-Reactive Co3 (PO4) 2 Nanoparticle Coating on High-Capacity LiNi0.8Co0.16Al0.04O2 Cathode Material for Lithium Rechargeable Batteries. *J. Electrochem. Soc.* **154**, A495–A499 (2007).
17. Cho, D.-H. *et al*. Effect of Residual Lithium Compounds on Layer Ni-Rich Li[Ni0.7Mn0.3]O2. *J. Electrochem. Soc.* **161**, A920–A926 (2014).
18. Arai, H., Okada, S., Ohtsuka, H., Ichimura, M. & Yamaki, J. Characterization and cathode performance of Li1 − xNi1 + xO2 prepared with the excess lithium method. *Solid State Ionics* **80**, 261–269 (1995).
19. Cho, S.-W., Kim, G.-O. & Ryu, K.-S. Sulfur anion doping and surface modification with LiNiPO4 of a Li[Co0.1Ni0.15Li0.2Mn0.55] O2 cathode material for Li-ion batteries. *Solid State Ionics* **206**, 84–90 (2012).
20. Liu, Y. *et al*. Li3V2(PO4)3-coated Li1.17Ni0.2Co0.05Mn0.58O2 as the cathode materials with high rate capability for Lithium ion batteries. *Electrochim. Acta* **147**, 696–703 (2014).
21. Choi, J. & Lee, J. Improved electrochemical properties of Li(Ni0.6Mn0.2Co0.2)O2 by surface coating with Li1.3Al0.3Ti1.7(PO4)3. *J. Power Sources* **307**, 63–68 (2016).
22. Appapillai, A. T., Mansour, A. N., Cho, J. & Shao-Horn, Y. Microstructure of LiCoO2 with and without 'AlPO4' Nanoparticle Coating: Combined STEM and XPS Studies. *Chem. Mater.* **19**, 5748–5757 (2007).
23. Jo, C.-H. *et al*. An effective method to reduce residual lithium compounds on Ni-rich Li[Ni0.6Co0.2Mn0.2]O2 active material using a phosphoric acid derived Li3PO4 nanolayer. *Nano Res.* **8**, 1464–1479 (2015).
24. Aykol, M., Kirklin, S. & Wolverton, C. Thermodynamic Aspects of Cathode Coatings for Lithium-Ion Batteries. *Adv. Energy Mater.* **4**, 1400690–n/a (2014).
25. Aykol, M. *et al*. High-throughput computational design of cathode coatings for Li-ion batteries. *Nat. Commun.* **7**, 13779 (2016).
26. Snydacker, D. H., Aykol, M., Kirklin, S. & Wolverton, C. Lithium-Ion Cathode/Coating Pairs for Transition Metal Containment. *J. Electrochem. Soc.* **163**, A2054–A2064 (2016).
27. Mosqueda, H. A., Vazquez, C., Bosch, P. & Pfeiffer, H. Chemical Sorption of Carbon Dioxide (CO2) on Lithium Oxide (Li2O). *Chem. Mater.* **18**, 2307–2310 (2006).
28. Park, K. *et al*. Re-construction layer effect of LiNi0.8Co0.15Mn0.05O2 with solvent evaporation process. *Sci. Rep.* **7**, 44557 (2017).
29. Min, K., Seo, S.-W., Choi, B., Park, K. & Cho, E. Computational screening for design of optimal coating materials to suppress gas evolution in Li-ion battery cathodes. *ACS Appl. Mater. Interfaces* **9**, 17822–17834 (2017).
30. Kresse, G. & Furthmüller, J. Efficient iterative schemes for ab-initio total energy calculations using a plane-wave basis set. *Phys. Rev. B* **54**, 11169–11186 (1996).
31. Kresse, G. & Furthmüller, J. Efficiency of ab-initio total energy calculations for metals and semiconductors using a plane-wave basis set. *Comput. Mater. Sci.* **6**, 15–50 (1996).
32. Heyd, J. & Scuseria, G. E. Efficient hybrid density functional calculations in solids: Assessment of the Heyd–Scuseria–Ernzerhof screened Coulomb hybrid functional. *J. Chem. Phys*. **121** (2004).
33. Heyd, J., Scuseria, G. E. & Ernzerhof, M. Hybrid functionals based on a screened Coulomb potential. *J. Chem. Phys*. **118** (2003).
34. Chase, M. W., of Standards, N. I. & (U.S.), T. *NIST-JANAF thermochemical tables*. ([Washington, D.C.]: American Chemical Society; Woodbury, N.Y.: American Institute of Physics for the National Institute of Standards and Technology, 1998).

Author Contributions

K. Min designed and performed the simulations and wrote the manuscript. E. Cho interpreted the data and wrote the manuscript. S. Seo analyzed and interpreted the data. K. Park, S. Park, and B. Choi performed the experiments and interpreted the data. All authors reviewed the manuscript.

Additional Information

Supplementary information accompanies this paper at doi:10.1038/s41598-017-07375-6

Competing Interests: The authors declare that they have no competing interests.

Publisher's note: Springer Nature remains neutral with regard to jurisdictional claims in published maps and institutional affiliations.